Quantum Noise in Differential-type Gravitational-Wave Interferometer and Signal Recycling

Atsushi Nishizawa[1], **Seiji Kawamura**[2], **Masa-aki Sakagami**[1]

[1] Graduate School of Human and Environmental Studies, Kyoto University, Kyoto 606-8501, Japan

[2] TAMA Project, National Astronomical Observatory of Japan, 2-21-1 Osawa, Mitaka, Tokyo 181-8588, Japan

E-mail: atsushi.nishizawa@nao.ac.jp

Abstract. There exists the standard quantum limit (SQL), derived from Heisenberg's uncertainty relation, in the sensitivity of laser interferometer gravitational-wave detectors. However, SQL can be overcome using the correlation of shot noise and radiation-pressure noise. So far, signal recycling, which is one of the methods to overcome SQL, is considered only in a recombined-type interferometer such as Advanced-LIGO, LCGT, and GEO600. In this paper, we investigated quantum noise and signal recycling in a differential-type interferometer. We also considered the application as a real detector and compared the sensivity with a recombined type.

1. Introduction

The first generation of kilometer-scale, ground-based laser interferometer gravitational-wave (GW) detectors has begun its search for GW radiation and has yielded scientific results [1, 2, 3, 4]. The development of interferometers of the next-generation, such as Advanced-LIGO [5] and LCGT [6, 7], is underway.

In the first-generation interferometers, we can ignore radiation-pressure noise because the laser power is low enough. In the next-generation interferometers, laser power is so high that radiation-pressure noise should be treated correctly in a fully quantum-mechanical way, in which the radiation-pressure noise could have the correlation with shot noise [8]. These two noises have different dependences on laser power I_0. The spectral density of radiation-pressure noise is proportional to I_0 and that of shot noise is inverse-proportional to I_0. Thus, there exists an optimal laser power to reach maximum sensitivity at a certain frequency. This maximum reachable sensitivity is called the standard quantum limit (SQL) [9, 10].

Nonetheless, it is possible to circumvent SQL by using signal recycling, which is one of the methods circumventing SQL and uses one extra mirror, called a Signal Recycling (SR) mirror[1]. This additional mirror can reshape the noise curve and make dips in it [11, 12]. Recently,

[1] The interferometer configuration is called signal recycling, detuned signal recycling or resonant sideband extraction, depending on the microscopic position of the extra mirror at the dark port. In this paper, however, we stick to the term "signal recycling" for convenience.

quantum noise has been calculated in the case of Advanced-LIGO, in which SR mirror is put at the dark port of the interferometer [13, 14]. SR mirror creates dynamical correlations between shot noise and radiation-pressure noise and this makes it possible to circumvent SQL. The signal recycling is planned to apply to the next-generation interferometers such as Advanced-LIGO and LCGT [5, 6]. These interferometers interfere two lights returning from two arms and detect a differential signal. This detection method is called recombined-type.

On the other hand, there exists another method called differential-type, which detects signals for each arm independently and combines (differentiates) them after the detection. In this configuration, however, one cannot increase laser power using a power-recycling mirror. This seems to be a fatal defect for a differential-type interferometer when it is applied to ground-based interferometers, because more laser power is needed to decrease shot noise. However, in our signal-recycling configuration described in this paper, the power recycling is possible with two SR mirrors located at the output. Thus, a differential-type interferometer could become a new design for future GW detectors. The aim of this paper is to investigate quantum noise and achievable sensitivity in differential-type interferometers with signal recycling.

2. Quantum noise in a differential-type interferometer

2.1. Conventional interferometer

Recently, full-quantum treatment of quantum noise has been formulated by Kimble *et al.* [8]. We will use the formalism and derive quantum noise in a conventional differential-type interferometer shown in Fig.1. Laser light entering the beam splitter (BS) is split into two directions and enters a pair of a polarization beam splitter (PBS) and a quarter wavelength ($\lambda/4$) plate at each arm. After being reflected by the FP cavity, the light is transmitted through the $\lambda/4$ plate and is reflected by PBS. Then the beams are detected at the photo detectors independently in each arm.

For simplicity, we assume that all optics (beam splitter, PBS, $\lambda/4$ plate and the mirrors of FP cavity) are lossless. The end mirrors of the FP cavity are completely reflective and its front mirrors have amplitude transmissivity T and reflectivity R [2]. The zeroth order length of the FP cavity satisfies resonant condition $L = n\lambda/2$; n is the integer and λ is the wavelength of carrier light. In this paper, we select $L = 3\,\mathrm{km}$.

Quantum noise is caused by vacuum field $\mathbf{a}$ (input field in this configuration) entering an interferometer from the dark port [15]. The field $\mathbf{a}$ is shot noise itself and also produces radiation-pressure noise, coupled with the carrier light in the Fabry-Perot (FP) cavity. "b^n " and "b^e " are the output field, where subscripts "n" and "e" denote "north" and "east", respectively. These fields include shot noise, radiation-pressure noise and GW signal.

The input-output relations can be obtained using optical junction conditions of beam splitters and mirrors. The detail calculation is described in [16]. As a result, we obtain the spectral density of noise in a conventional differential-type interferometer,

$$S_h(\Omega) = \frac{h_{\mathrm{SQL}}^2}{2}\left(\frac{1}{K} + K\right) . \tag{1}$$

Various quantities are defined as below,

$$\gamma = \frac{T^2 c}{4L} , \qquad \beta(\Omega) = \arctan(\Omega/\gamma) , \qquad I_{\mathrm{SQL}} = \frac{mL^2\gamma^4}{4\omega_o},$$

$$K(\Omega) = \frac{2(I_0/I_{\mathrm{SQL}})}{(\Omega/\gamma)^2[1 + (\Omega/\gamma)^2]}, \qquad h_{\mathrm{SQL}}(\Omega) = \sqrt{\frac{8\hbar}{m\Omega^2 L^2}} ,$$

[2] This is different from the definition in KLMTV's paper.

where c is the speed of light, $\hbar$ is the reduced Planck constant, $\omega_0\,(=1.8\times10^{15}\,\mathrm{rad/sec})$ is the angular frequency of a laser, $m\,(=30\,\mathrm{kg})$ is mass of a mirror, γ is FP-cavities' half bandwidth, which determines the characteristic frequency of the FP cavity, and β is the effective phase shift of a sideband field in the FP cavity. K is a coupling constant between a carrier field and a sideband field, which depends laser power I_0 and determines the intensity of radiation-pressure. h_{SQL} is the square root of the SQL spectral density and I_{SQL} is the laser power required to reach SQL at $\Omega=\gamma$.

Equation (1) is the same formula as that in the recombined-type [8] and reaches SQL at $\Omega=\gamma$ when the laser power I_0 is I_{SQL}. However, it does not overcome SQL. The reason is that shot noise and radiation pressure noise have no dynamical correlation. Therefore, they give the achievable minimum noise level. In a conventional differential-type interferometer, it is impossible to implement power recycling. Therefore, there seems to be no advantage in using a conventional differential-type interferometer instead of a conventional recombined-type one, from the point of view of the sensitivity.

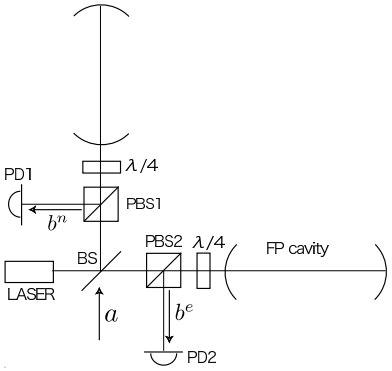

Figure 1. Conventional configuration of differential-type interferometer, and input and output fields.

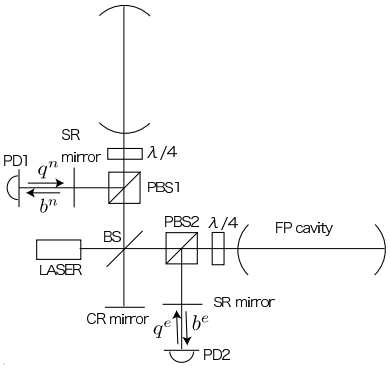

Figure 2. SR configuration of a differential-type interferometer and input and output fields.

2.2. Signal recycling

Signal recycling in a recombined-type GW interferometer has been investigated by Buonanno and Chen [13, 14]. The SR mirror is located at the dark port (differential output port) of the interferometer. The outgoing signal from the beam splitter is reflected by the SR mirror and reenters the interferometer with some phase shift in the SR cavity. Then, the signal circulates in the interferometer many times and creates the resonances at certain frequencies. As a result, the noise curve has two dips at the resonant frequencies, which overcome the SQL.

These two dips have different origins. One corresponds to an optical resonance (sideband resonance) and the other corresponds to a mechanical resonance (optical rigidity). The optical resonance is just the resonance in the cavities due to the sideband fields. On the other hand, the mechanical resonance has the origin in the suspension system. When the laser power is high, the resonant frequency is shifted upward into the detection band by the optical rigidity, which is caused by the nontrivial coupling between radiation pressure and mirror motion. In the case with detuned SR phase, the mirror no longer behaves like a free mass, but like a mass attached to a mechanical spring due to optical fields.

In this subsection, we will consider the signal-recycling configuration of a differential-type interferometer. To implement this, SR mirrors should be put just in front of the photo detectors.

We also need to put completely reflecting mirror (CR mirror) at the dark port to close the entire system. Thus, vacuum fields coming into the interferometer from outside are only **q** fields. This interferometer configuration has two important parameters $\phi \equiv [\omega_0 \ell_s/c]_{\mathrm{mod}\ 2\pi}$ and $\theta \equiv [\omega_0 \ell_d/c]_{\mathrm{mod}\ 2\pi}$, where ℓ_s and ℓ_d are the lengths of the SR cavity and the dark port cavity. More strictly, these are the distances between the PBS and the SR mirror and between the beam splitter and the CR mirror, respectively. We assume these lengths are small compared with the FP cavity's arm length L ($\ell_s,\ \ell_d\ \sim$ several meters). Thus, phase shifts for sideband in these cavities are negligible and we will ignore them hereafter. ϕ has to be set to the same value for both arms, otherwise the common mode of noise signal contributes to the final differential signal and worsens the sensitivity. Amplitude reflectivity and transmissivity of the SR mirror are ρ and τ, respectively.

The spectral density of noise in this configuration can be derived after lengthy but straightforward calculations described in [16], is given by,

$$S_h = \frac{h_{\mathrm{SQL}}^2}{2K\tau^2}\frac{(C_{11}\sin\zeta + C_{21}\cos\zeta)^2 + (C_{12}\sin\zeta + C_{22}\cos\zeta)^2}{|D_1\sin\zeta + D_2\cos\zeta|^2}, \tag{2}$$

$$\begin{aligned} C_{11} &= (1+\rho^2)\ \cos 2(\theta+\phi) - 2\rho\ \cos 4\beta \\ &\quad + \frac{K}{2}\left[(1+\rho^2)^2\ \sin 2(\theta+\phi) - \tau^4\ \sin 2\theta + 2\rho\ \cos 2\beta\{(1+\rho^2)\ \sin 2\phi + 2\rho\ \sin 2\theta\}\right] \end{aligned} \tag{3}$$

$$\begin{aligned} C_{22} &= (1+\rho^2)\ \cos 2(\theta+\phi) - 2\rho\ \cos 4\beta \\ &\quad + \frac{K}{2}\left[(1+\rho^2)^2\ \sin 2(\theta+\phi) + \tau^4\ \sin 2\theta + 2\rho\ \cos 2\beta\{(1+\rho^2)\ \sin 2\phi + 2\rho\ \sin 2\theta\}\right] \end{aligned} \tag{4}$$

$$C_{12} = -\tau^2\left[\sin 2(\theta+\phi) + K\ \sin\phi\ \{(1+\rho^2)\ \sin(2\theta+\phi) + 2\rho\ \cos 2\beta\ \sin\phi\}\right] \tag{5}$$

$$C_{21} = \tau^2\left[\sin 2(\theta+\phi) - K\ \cos\phi\ \{(1+\rho^2)\ \cos(2\theta+\phi) + 2\rho\ \cos 2\beta\ \cos\phi\}\right] \tag{6}$$

$$D_1 = -\left[(1+\rho^2 e^{6i\beta})\ \sin\phi + 2\rho\, e^{3i\beta}\ \cos\beta\ \sin(2\theta+\phi)\right] \tag{7}$$

$$D_2 = -\left[(-1+\rho^2 e^{6i\beta})\ \cos\phi + 2i\rho\, e^{3i\beta}\ \sin\beta\ \cos(2\theta+\phi)\right]\ . \tag{8}$$

C_{ij} and D_i involve the contribution of quantum noise and GW signal, respectively. In the above equations, the effective phase shift in the FP cavity doubles compared with that of the recombined-type because the differential-type SR interferometer effectively has two FP cavities when light goes around the interferometer and this extends the length of the light path in the interferometer.

A characteristic sensitivity curve of a differential-type SR interferometer for certain parameters is drawn in Fig.3. There appears three dips and one GW signal suppression peak. The important thing here is that these three dips overcome the SQL. In comparison with a recombined-type, there appears one additional dip. In [16], we analyzed the behavior of dips in detail and found that one of dips has mechanical origin and others have optical origin. This is because the light passes through the FP cavity twice when it goes around a differential-type interferometer. In other words, two FP cavities are coupled. This allows the sideband field to increase the resonant solution. Strictly speaking, in the case of a recombined-type, two sidebands $\pm\Omega$ satisfy the same condition and have degenerated resonant frequencies, while, in a differential-type, asymmetric resonant conditions allow two sidebands $\pm\Omega$ to have different resonant frequencies.

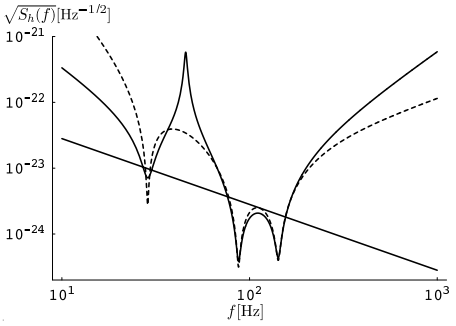

Figure 3. Characteristic sensitivity curve of differential-type SR interferometer. Parameters selected are $T = 0.14$, $\rho = 0.98$, $I_0 = I_{SQL}$, $\phi = 1.4$, $\theta = 0.86$. Solid curve is the sensitivity of quadrature mode 1 ($\zeta = \pi/2$) and dashed curve is that of quadrature mode 2 ($\zeta = 0$). Diagonal black line is h_{SQL}.

3. Application of differential-type SR interferometer to real GW interferometer

In this section, we will consider the application of our configuration to a real GW interferometer and compare it with the next-generation ground-based interferometers such as Advanced-LIGO [5] and LCGT [7]. They have much better goal sensitivity than the present detectors in operation and almost all frequency bands are limited by quantum noise. This means that it would be possible to improve the sensitivity by reshaping the quantum noise. For the comparison, we should take into account not only quantum noise but also classical noise, that is, thermal and seismic noise. Thus, we will compare the SNR of a differential-type for NS-NS binary or BH-BH binary with that of a recombined-type.

For the comparison, we will fix the injected laser power to $I_0 = 996$ W for the comparison with LCGT and $I_0 = 1284$ W for the comparison with Advanced-LIGO. These laser powers effectively include power recycling gain and are determined to have the same laser powers in the FP cavity, 780 kW for LCGT and 803 kW for Advanced-LIGO, as in the design document [7, 5], with the reflectivity of the FP cavity's mirror in the documents. This is because the laser power in the FP cavity is most important for quantum noise. Then, we selected $T = 0.14$ corresponding to $I_{SQL} \approx 2200$ W. We explored other parameters of a differential-type SR interferometer over all parameter space and finally selected two sets of parameters for the comparison with LCGT and one set for the comparison with Advanced-LIGO, to decrease quantum noise at low frequencies keeping the moderate sensitivity in high frequency. All parameters are listed in Table 1. The sensitivity curves are shown in Fig.4 and Fig.5 including Advanced-LIGO and LCGT design sensitivity and other classical noise.

SNR of a inspiral binary is given by the formula [17],

$$(SNR)^2 = 4\int_0^\infty df \frac{|\hat{h}(f)|^2}{S_h(f)} \tag{9}$$

where $\hat{h}(f)$ is the Fourier component of GW amplitude and is proportional to $f^{-7/6}$ for an inspiral binary. Using this formula, one can calculate the SNR of the sensitivity curves given in Fig.4 and Fig.5. However, observed frequency band for an inspiral binary is limited since it will begin to merge at the frequency corresponding to an innermost stable circular orbit [17]. Thus, we calculated SNRs for three cases; (i) $1.4M_\odot$-$1.4M_\odot$ NS binary (full integration range of frequency), (ii) $50M_\odot$-$50M_\odot$ BH binary (limited to $f < 80$ Hz), and (iii) $100M_\odot$-$100M_\odot$ BH binary (limited to $f < 40$ Hz). The results are summarized in Table 1.

In the case of Advanced-LIGO, classical noise prevents the sensitivity from improving much because the magnitude of quantum noise is comparable with that of classical noise (Fig.4). Nevertheless, SNR is improved slightly due to the third dip when the integrated frequency range is limited at low frequencies. Comparing the Advanced-LIGO, the ratio of SNR is improved by the factor of 1.24 for $100M_\odot$ BH binary. On the other hand, LCGT has the thermal noise

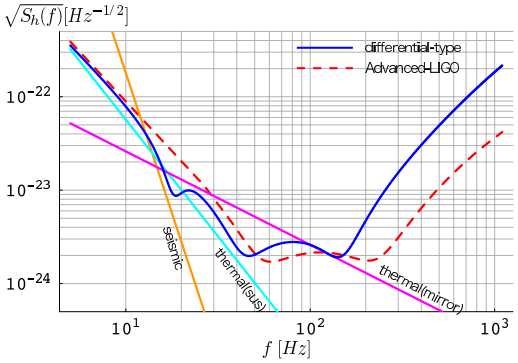

Figure 4. Comparison of the sensitivity curves of a differential-type SR interferometer and Advanced-LIGO. Solid and dashed curve are the sensitivity curve of the differential-type with adjusted parameters listed in Table 1 and Advanced-LIGO. Other classical noises are also plotted [5].

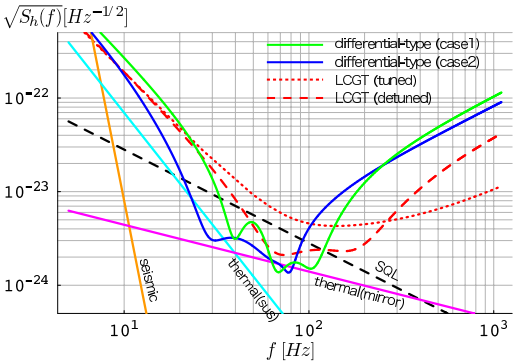

Figure 5. Comparison of the sensitivity curves of a differential-type SR interferometer and LCGT. Two solid curves are the sensitivity curves of the differential-type with adjusted parameters listed in Table 1. Dotted and dashed curves are the sensitivity curves of LCGT with tuned and detuned configuration, respectively. Other classical noises are also plotted [7].

Table 1. List of parameters and SNR sensitivity for LCGT, Advanced-LIGO and a differential-type. The values of SNR sensitivity in this table are defined as normalized SNR by that of Advanced LIGO and LCGT (tuned).

configuration	T	ρ	ϕ	θ	ζ	NS - NS	BH - BH ($50M_\odot$)	BH - BH ($100M_\odot$)
Advanced-LIGO	0.0707	0.96	1.51	—	$\pi/2$	1	1	1
Differential-type	0.1400	0.78	1.09	1.32	$\pi/2$	0.90	1.05	1.24
LCGT (tuned)	0.0632	0.88	$\pi/2$	—	$\pi/2$	1	1	1
LCGT (detuned)	0.0632	0.95	1.49	—	0.80	1.25	1.56	1.17
Differential-type (case1)	0.1400	0.85	1.38	0.61	2.74	1.30	1.87	1.81
Differential-type (case2)	0.1400	0.59	0.13	1.49	1.00	1.43	2.28	2.94

relatively smaller than that of Advanced-LIGO due to cryogenic technique. Seismic noise is also smaller because LCGT is built underground. In the case of differential-type (case2), the SNR is improved by the factor 1.43 for NS binary, 2.28 for $50M_\odot$ BH binary and 2.94 for $100M_\odot$ BH binary, compared with the SNR of LCGT (tuned). For reference, we also show the sensitivity of LCGT(detuned). Two differential-type (case1 and case2) still have better sensitivity compared with LCGT (detuned). Thus, we can conclude that a differential-type has better sensitivity at low frequencies and more advantage than a recombined-type from the point of view of quantum noise .

At the end of this section, we will mention the laser power needed to realize the sensitivity and the power recycling. In the calculation, we fixed the laser power $I_0 = 996$ W for the comparison with LCGT and $I_0 = 1284$ W for the comparison with Advanced-LIGO. For recombined-type,

these laser powers are obtainable using power recycling. For a differential-type, however, these laser power is slightly large. The reason is that power recycling is possible in our differential SR configuration due to SR mirrors, however, SR mirror's reflectivity limits the recycling gain. In other words, the some fraction of carrier light is lost at the SR mirrors. Therefore, several handreds watt laser is needed to achieve the laser power used in this paper. The power-recycling gain is not problematic if one uses a high reflective SR mirror. Further detailed investigation should be done on this matter.

4. conclusion and future work

Our purpose in this paper is investigating the advanced designs of GW detectors. We extended signal recycling scheme in a recombined-type interferometer to a differential-type. In this detector design, there appears three dips on the noise curve, where two dips are optical resonance and one dip is mechanical resonance. Taking advantage of this additional dip, we can obtain sensitivity better than that of a recombined-type. We found that the SNRs for inspiral binaries are improved by a factor of ≈ 1.43 for NS binary, ≈ 2.28 for $50M_{\odot}$ BH binary and ≈ 2.94 for $100M_{\odot}$ BH binary compared with LCGT. Therefore, a differential-type interferometer has more advantage than recombined-type and could become a candidate for the third-generation GW interferometer, though the laser power is slightly large.

In the theoretical consideration in this paper, there are some practical issues that we did not consider. What should be considered is (i) lock acquisition scheme to operate a differential-type SR interferometer, (ii) loss effects of all optics, (iii) instability of a system and ways of dealing with it. Answering these questions is future work for the implementation of a differential-type SR interferometer as a real detector.

Acknowledgments

We wish to acknowledge Y. Chen, M. Ando, and S. Sato for useful discussion and comments, and R. Adhikari and T. Corbitt for useful imformation about Advanced LIGO's parameters. We also acknowledge the support of the United States National Science Foundation for the construction and operation of the LIGO Laboratory.

References

[1] Waldman S J *et al.* 2006 *Class. Quantum. Grav.* **23** S653
[2] Acernese F *et al.* 2006 *Class. Quantum. Grav.* **23** S635
[3] Hild S *et al.* 2006 *Class. Quantum. Grav.* **23** S643
[4] Ando M *et al.* 2001 *Phys. Rev. Lett.* **86** 3950
[5] Advanced LIGO webpage; http://ilog.ligo-wa.caltech.edu:7285/advligo/, http://www.ligo.caltech.edu/ ligo2/pdf/sapphiresilicaref.pdf
[6] LCGT webpage; http://www.icrr.u-tokyo.ac.jp/gr/
[7] LCGT internal document
[8] Kimble H J, Levin Y, Matsko A B, Thorne K S and Vyatchanin S P 2001 *Phys. Rev.* D **65** 022002
[9] Braginsky V B and Khalili F Y 1992 *Quantum mesurement* (Cambridge University Press)
[10] Braginsky V B, Gorodetsky M L, Khalili F Y, Matsko A B, Thorne K S and Vyatchanin S P 2003 *Phys. Rev.* D **67** 082001
[11] Meers B J 1988 *Phys. Rev.* D **38** 2317
[12] Mizuno J, Strain K A, Nelson P G, Chen J M, Schilling R, Rudiger A, Winkler W and Danzmann K 1993 *Phys. Lett.* A **175** 273
[13] Buonanno A and Chen Y 2001 *Phys. Rev.* D **64** 042006
[14] Buonanno A and Chen Y 2002 *Phys. Rev.* D **65** 042001
[15] Caves C M 1981 *Phys. Rev.* D **23** 1693
[16] Nishizawa A, Kawamura S and Sakagami M 2007 *Phys. Rev.* D **76** 042002
[17] Flanagan E E and Hughes S A 1998 *Phys. Rev.* D **57** 4535